J|A|C|S
ARTICLES
Published on Web 05/27/2007

Cyclization Cascade of Allenyl Azides: A Dual Mechanism

Carlos Silva López,*[,†,‡] Olalla Nieto Faza,[†,‡] Ken S. Feldman,[§] Malliga R. Iyer,[§] and D. Keith Hester II[§]

Contribution from the Departamento de Quimica Organica, Universidade de Vigo, Lagoas Marcosende, 36200, Vigo, Galicia, Spain, Department of Chemistry, University of Minnesota, 207 Pleasant Street SE, Minneapolis, Minnesota 55455-0431, and Department of Chemistry, The Pennsylvania State University, 104 Chemistry Building, University Park, Pennsylvania 16802

Received February 5, 2007; E-mail: silva@chem.umn.edu; csilval@uvigo.es

Abstract: A density functional theory based computational approach to describing the mechanistic course of the allene azide cycloaddition cascade sequence has been developed. The results of these calculations permit characterization of key reactive intermediates (diradicals and/or indolidenes) and explain the different behaviors observed in the experimental studies between conjugated and nonconjugated species. Furthermore, computational analysis of certain intermediates offer insight into issues of regioselectivity and stereoselectivity in cases where different reaction channels are in competition, suggesting suitable substitutions to achieve a single regioisomer in the indole synthesis via azide−allene cyclization.

1. Introduction

The construction of core C−C bonds in sterically hindered environments remains an enduring challenge in complex molecule synthesis. Toward this end, cyclization reactions that proceed through diradical closures offer the promise of facile bond formation in congested locations as a consequence of the typically minimal activation barriers for diyl union compared with heteropolar and/or closed-shell alternatives. However, the development of diradical cyclization chemistry has been hampered by the rather limited collection of synthesis methods that can generate diyl intermediates. One recent advance in this area emerged upon exploration of the thermochemistry of 5-azidoallenes, exemplified by **1** and **8** and their aryl analogues $\mathbf{1}_{Ph}$ and $\mathbf{8}_{Ph}$ (Figure 1).[1,2] Mild heating (110 °C) of these substrates initiated a cascade sequence postulated to proceed through (i) initial allene/azide [3 + 2] cycloaddition, (ii) N_2 loss from the intermediate triazoline to afford a diyl, and (iii) diyl cyclization through the appended unsaturation (alkene or arene) to furnish the closed shell products **4/6** and **12/13/14**, respectively.

The putative intermediate (singlet) diyls **3**, $\mathbf{3}_{Ph}$ and **10**, $\mathbf{10}_{Ph}$ have the options of closure to form either C−C bonds (→ **4/6** or **12**, respectively) or C−N bonds (→ **5/7** or **13**, respectively) from both the unconjugated **1**, $\mathbf{1}_{Ph}$ and conjugated **8**, $\mathbf{8}_{Ph}$ substrates. In addition, the conjugated substrates **8** and $\mathbf{8}_{Ph}$ present a distinct and alternative option to diyl chemistry; reaction through the closed shell 2-indolidene intermediate **11** and $\mathbf{11}_{Ph}$. This putative intermediate might arise either by bond rotation/electronic reorganization of a first-formed (singlet) diyl **10**, $\mathbf{10}_{Ph}$ or by direct N_2 extrusion from the triazoline **9** and $\mathbf{9}_{Ph}$, respectively. The preliminary reports of this chemistry did not provide any evidence that permits a distinction to be made between these mechanistic options.

A thorough computational study of these systems is described in this report. By dissecting these cascade processes into their component steps and comparing the relative activation barriers of these steps, insight into the following questions can be garnered:

- Why does the unconjugated substrate **1** yield only the C−C bonded product **4** upon thermolysis, whereas the conjugated analogue **8** provides both C−C **12** and C−N **13** bonded products in roughly equal amounts?
- Which intermediate, the diyl **10** or the closed shell alternative **11**, is formed first from **9**, and which of these species is the direct precursor to the tetracyclic products **12/13**?
- What is the basis for the strictly cis stereochemical outcome upon cyclization of diyl **3** to form **4**?
- Why do the alkenyl-bearing substrates **8** yield tetracycle through participation of the alkene, whereas the aryl-bearing analogue $\mathbf{8}_{Ph}$ does not engage the aryl ring in C−C bond formation but rather forms a simple 2-styrylindole product **14**?

This study will disclose the key steps of the cascade process responsible for the observed stereocontrol and regiocontrol. Moreover, the detailed description of the reaction profiles for the formation of the two regioisomers **12** and **13** from **8** may form the basis for developing strategies to steer the reaction toward one product or the other.

2. Computational Methods

The density functional theory[3] in its Kohn−Sham[4] formulation was employed throughout this work. All of the stationary points were computed with B3LYP,[5] a three-parameter hybrid[6] functional combining

[†] Universidade de Vigo.
[‡] University of Minnesota.
[§] The Pennsylvania State University.

(1) Feldman, K. S.; Iyer, M. R. *J. Am. Chem. Soc.* **2006**, *127*, 4590−4591.
(2) Feldman, K. S.; Iyer, M. R.; Hester, D. K., II. *Org. Lett.* **2006**, *8*, 3113−3116.
(3) Hohenberg, P.; Kohn, W. *Phys. Rev.* **1964**, *136*, B864−B871.
(4) Kohn, W.; Sham, L. *Phys. Rev. A* **1965**, *140*, A1133−A1138.

10.1021/ja070818l CCC: $37.00

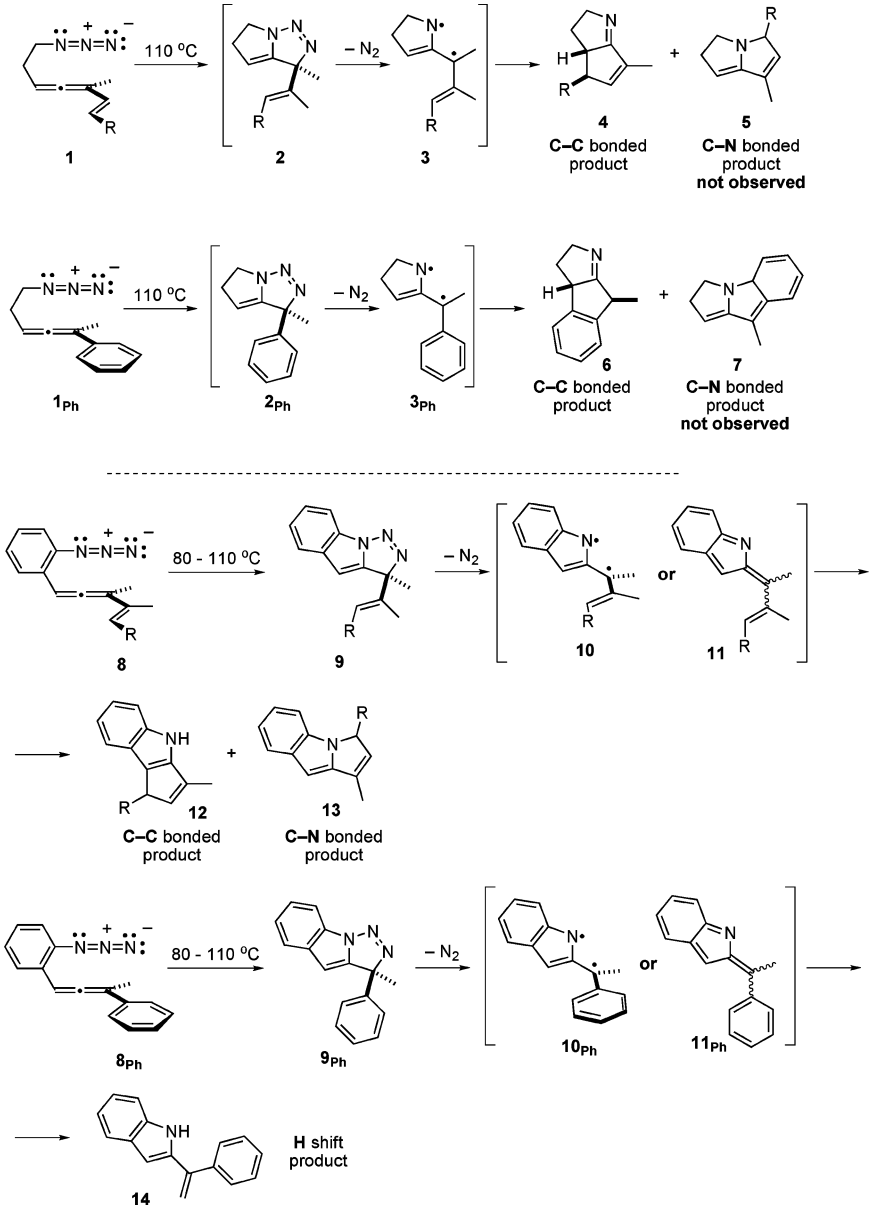

Figure 1. Preliminary results and mechanistic speculation for the azide−allene cyclization cascade sequence.

the 1988 exchange functional by Becke[7] with the correlation functional by Lee, Yang, and Parr[8] as implemented in Gaussian03.[9] A dual level scheme was used to ensure high quality in the computed values. Geometry optimization and frequencies were computed with the 6-31G(d,p) basis set, and further energy refinement and properties were computed with the split-valence, triple-ζ, 6-311+G(d,p) basis set. This scheme usually is noted as B3LYP/6-311+G(d,p)//B3LYP/6-31G(d,p). Diffuse functions were included in this methodological scheme, as some structures exhibited large localized negative partial charges in preliminary results. The choice of DFT and the Pople basis sets is backed by earlier studies in which this method offered reasonable results at a moderate cost despite the presence of diradical species in the reaction profile.[10−12]

Due to the potential diradical character of some of the structures considered in this work, the internal and external stability of the wavefunctions was computed via the Hermitian stability matrices **A** and **B** in all cases.[13] For all the structures exhibiting unstable restricted wavefunctions, the spin-symmetry constraint of the wavefunction was released (i.e., expanding the SCF calculation to an unrestricted space, UB3LYP), leading to stable unrestricted wavefunctions.

As a test of the method, the activation energies for several known complementary diyl formation reactions were computed; very good agreement with experiment was observed in all cases (see Supporting Information).

Nucleus independent chemical shifts (NICS)[14] and the anisotropy of the current induced density (ACID)[15] were evaluated using the gauge-

(5) Stephens, P. J.; Devlin, F. J.; Chabalowski, C. F.; Frisch, M. J. *J. Phys. Chem.* **1994**, *98*, 11623−116237.
(6) Becke, A. D. *J. Chem. Phys.* **1993**, *98*, 5648−5652.
(7) Becke, A. D. *Phys. Rev. A* **1988**, *38*, 3098−3100.
(8) Lee, C.; Yang, W.; Parr, R. G. *Phys. Rev. B* **1988**, *37*, 785−789.
(9) Frisch, M. J., et al. *Gaussian 03*, revision C.02; Gaussian, Inc.: Wallingford, CT, 2004.
(10) Hess, B. A., Jr.; Eckart, U.; Fabian, J. *J. Am. Chem. Soc.* **1998**, *120*, 12310−12315.
(11) Hess, B. A., Jr.; Smentek, L.; Brash, A. R.; Cha, J. K. *J. Am. Chem. Soc.* **1999**, *121*, 5603−5604.
(12) Lopez, C. S.; Faza, O. N.; York, D. M.; de Lera, A. *J. Org. Chem.* **2004**, *69*, 3635−3644.
(13) Bauernschmitt, R.; Ahlrichs, R. *J. Chem. Phys.* **1996**, *22*, 9047−9052.
(14) Schleyer, P. v. R.; Maerker, C.; Dransfeld, A.; Jiao, H.; Hommes, N. J. R. v. E. *J. Am. Chem. Soc.* **1996**, *118*, 6317−6318.
(15) Herges, R.; Geuenich, D. *J. Phys. Chem. A* **2001**, *105*, 3214−3220.

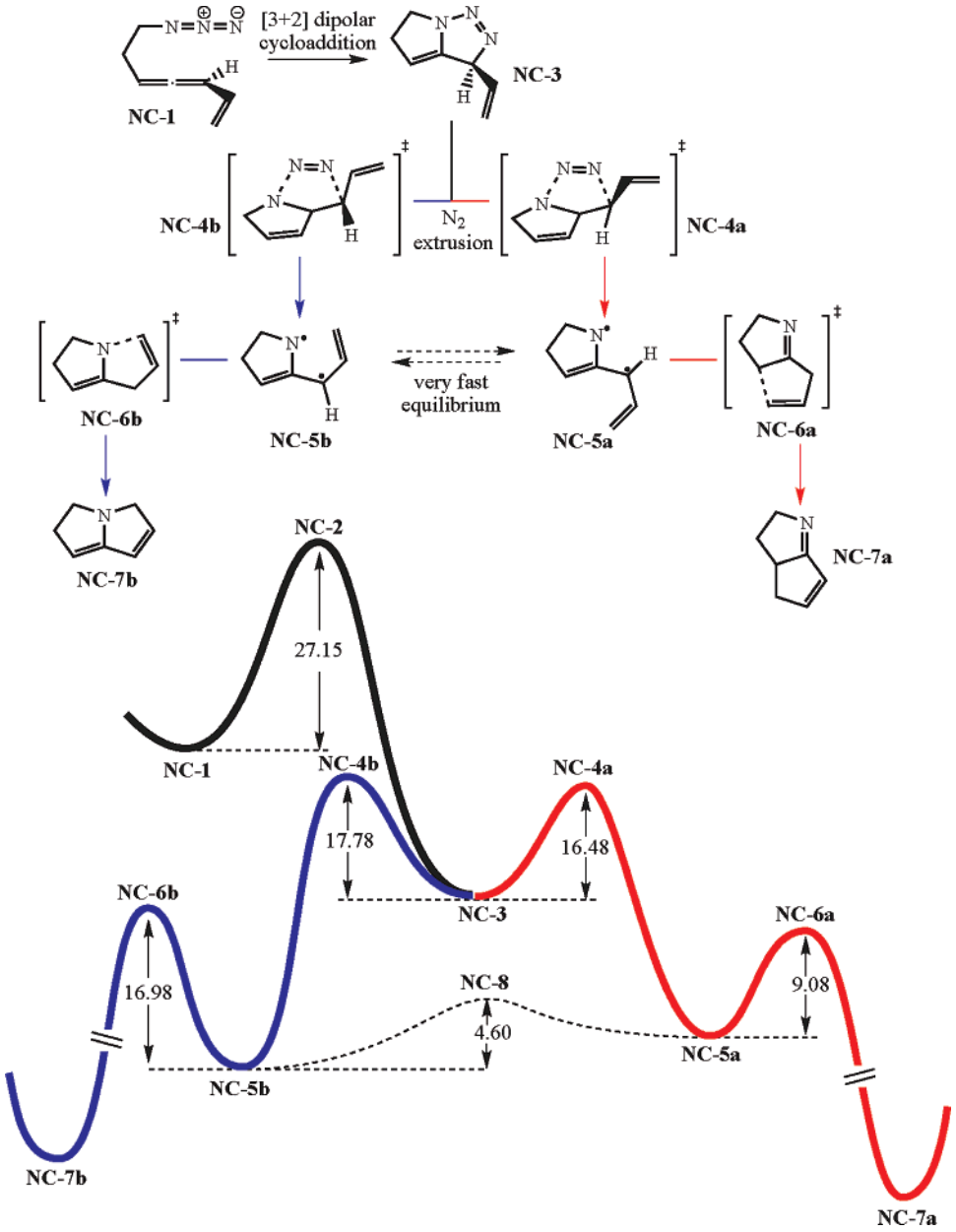

Figure 2. Mechanistic profile for the reaction cascade of nonconjugated allenyl azides.

independent atomic orbitals (GIAO)[16] and the continuous set of gauge transformations (CSGT),[17] respectively, to help describe whether the transition states exhibit aromatic character. Solvation effects on relative energies have been taken into account with the polarizable continuum model (PCM) in cases where comparisons to experiment required it.[18−20]

Complete active space SCF (CASSCF) calculations were performed with the 6-31G(d) basis set to accurately describe the diradical character of several key intermediates. These calculations were performed with the GAMESS package.[21] The active space in the CASSCF calculations presented in this work include the entire π system of the diyl intermediate, resulting in a six-electrons-in-six-orbitals active space, usually noted CASSCF(6,6).

3. Results and Discussion

3.1. Nonconjugated Allenyl Azides. 3.1.1. Mechanism of the Reaction Cascade. The cascade reaction sequence occurring under thermal activation yields a single product (**4** or **6**, depending on the starting material) when the azide and allene moieties are not connected through conjugation (cf. reactants **1** and $\mathbf{1}_{Ph}$ in Figure 1). Moreover, the reaction proceeds with complete stereocontrol to furnish a single diastereomer of bicyclic product **4**. This degree of control is surprising in light of the typically modest levels of diastereoselectivity reported to attend diradical collapse in other systems.[22]

Calculations on the model system **NC-1** (Figure 2) provide support for the preliminary mechanistic picture proposed in

(16) Wolinski, K.; Hinton, J. F.; Pulay, P. *J. Am. Chem. Soc.* **1990**, *112*, 8251−8260.
(17) Keith, T. A.; Bader, R. F. W. *Chem. Phys. Lett.* **1993**, *210*, 223−231.
(18) Tomasi, J.; Persico, M. *Chem. Rev.* **1994**, *94*, 2027−2094.
(19) Mineva, T.; Russo, N.; Sicilia, E. *J. Comput. Chem.* **1998**, *19*, 290−299.
(20) Cossi, M.; Scalmani, G.; Rega, N.; Barone, V. *J. Chem. Phys.* **2002**, *117*, 43−54.
(21) Schmidt, M. W.; Baldridge, K. K.; Boatz, J. A.; Elbert, S. T.; Gordon, M. S.; Jensen, J. H.; Koseki, S.; Matsunaga, N.; Nguyen, K. A.; Su, S.; Windus, T. L.; Dupuis, M.; A. Montgomery, J., Jr. *J. Comput. Chem.* **1993**, *14*, 1347−1363.
(22) Davidson, E. R.; Gajewski, J. J.; Shook, C. A.; Cohen, T. *J. Am. Chem. Soc.* **1995**, *117*, 8495−8501.

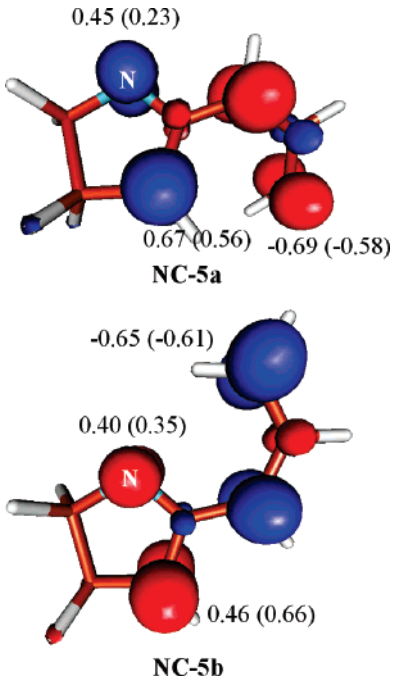

Figure 3. Isosurface of the spin density (0.02 e) at the diyl intermediates **NC-5a** and **NC-5b**. Values are the Mulliken spin density at the intermediate geometry and at the corresponding transition state geometry (in parentheses) in atomic units.

earlier work.[1] The first step is rate-limiting and involves a [3 + 2] dipolar cycloaddition of the azide moiety to the distal allene alkene (see Figure 2), a process whose activation energy is computed to be 27.2 kcal/mol. All the remaining steps toward the imine **NC-7a** are much more affordable in terms of activation energies. The triazoline **NC-3** releases nitrogen very easily (16−17 kcal/mol), yielding two isomeric diyls **NC-5a** and **NC-5b** that potentially could undergo cyclization to form two products, **NC-7a** and **NC-7b**, respectively. However, two mechanistic features favor convergence from both isomeric diyls. First, a very fast equilibrium which interconverts diyls **NC-5a** and **NC-5b** is available (4.6 kcal/mol). Second, the cyclization of **NC-5a** via transition state **NC-6a** to furnish the C−C bonded product **NC-7a** is much faster than the cyclization of its isomeric diyl to yield the C−N bonded product **NC-7b**. As a consequence, it is arguable that diyl **NC-5b** formed by nitrogen extrusion from the triazoline **NC-3** undergoes isomerization to **NC-5a** and then cyclization to **NC-7a** via transition state **NC-6a**.

3.1.2. Regio- and Stereochemistry. Closure of the diyl intermediates appears to strongly favor the transition state **NC-6a** to form a C−C single bond. That this transition state is substantially lower in energy than the alternative **NC-6b** can be traced to two features: (1) the greater stability of the C−C bond formed from **NC-6a** is felt to some extent in **NC-6a**, lowering its energy relative to **NC-6b**, and (2) the spin density is considerably larger on carbon compared to nitrogen in **NC-6a** and its predecessor **NC-5a** (see Figure 3). Note that the latter point is also compatible with the results of a frontier orbital analysis,[23] taking into account that carbon exhibits a larger orbital coefficient than nitrogen.

(23) Cichra, D. A.; Duncan, C. D.; Berson, J. A. *J. Am. Chem. Soc.* **1980**, *102*, 6527−6533.
(24) HOMO: Highest Occupied Molecular Orbital. LUMO: Lowest Unnoccupied Molecular Orbital. SOMO: Singly Occupied Molecular Orbital.

An explanation for the high stereoselectivity observed upon C−C bond formation from **NC-5a** can be found in a surprising place, the Woodward−Hoffmann (W−H) rules for ring closure. Even though this system is neither a [4*n*] nor a [4*n* + 2] π-electron system, the calculations detailed below provide a rationale for the closure of this formal 5-electron array that shares theoretical underpinnings with the venerable W−H dogma. A hint that electronic (orbital) control of stereochemistry might be paramount can be found in earlier calculations on the isoelectronic vinyl oxyallyl diyl system, which showed that this diyl system could be visualized as two disconnected radical species: an allyl fragment and an enol radical.[12] Complete active space SCF (CASSCF) calculations were performed for the ring closure transition state **NC-6a**. In addition, similar calculations with the alternative transition state **NC-6b** were quite revealing as well, even though it is unlikely that this species plays a role in product formation (vide supra). This methodology allows for a reliable orbital analysis of the diradical electronic structure in order to identify the source of stereoselectivity. The natural orbitals computed at the CASSCF level are illustrated in Figure 4. Strikingly, transition state **NC-6a** is found to conrotate toward the product **NC-7a**, whereas its C−N bond-forming counterpart **NC-6b** undergoes disrotatory motion toward **NC-7b**. This divergence of motion suggests that a W−H-like frontier orbital interaction might be governing the transition state character in both cases. Apparently, the polarization of the electron density caused by the electronegative nitrogen atom leads to C−C bond-forming ring closure via an electron-deficient five-electron system. Similarly, any C−N ring closure would have had to proceed through an electron-enriched cyclic structure. Therefore, the observed C−C bond formation to give **NC-7a** should resemble a four-electron cyclization, whereas the hypothetical C−N bond formation (**NC-7b**) is more similar to a six-electron cyclization in the classical W−H nomenclature. All the CASSCF natural orbitals in the active space are fully consistent with this view and present the appropriate number of phase changes for a four-electron conrotatory and a six-electron disrotatory ring closure, respectively (see Figure 4).

3.2. Conjugated Allenyl Azides. 3.2.1. Mechanism of the Reaction Cascade. Bridging the allene and azide moieties by an aryl group (cf. **8**, Figure 1) dramatically changes the nature of the intermediates and as a consequence the outcome of the reaction cascade, which now yields two regioisomers (**12** and **13** in Figure 1). The first steps are very similar to those postulated for the disconnected reactant **1**. Using model system **C-1** for computational efficiency, the initial [3 + 2] dipolar cycloaddition, now appears to proceed with concomitant six-electron hetero-electrocyclic closure to form the bicyclic core of **C-3** (see Figure 5). In marked contrast to the earlier nonconjugated series, the subsequent nitrogen extrusion does not yield a diyl. The extrusion reaction now leads to a pair of closed-shell heterocyclic products **C-5a** and **C-5b**. These calculations indicate that the barrier to interconversion between these geometrical isomers (via orthogonal diyl **C-8**) cannot be surmounted under the experimental conditions, and so they are formed and exist as discrete and independent species. Both regioisomers **C-5a** and **C-5b** then undergo electrocyclic ring closures (ERCs) independently to yield **C-7a** and **C-7b**, respectively. In this last and strongly exergonic step, rearomatization of the arene group provides a substantial driving force

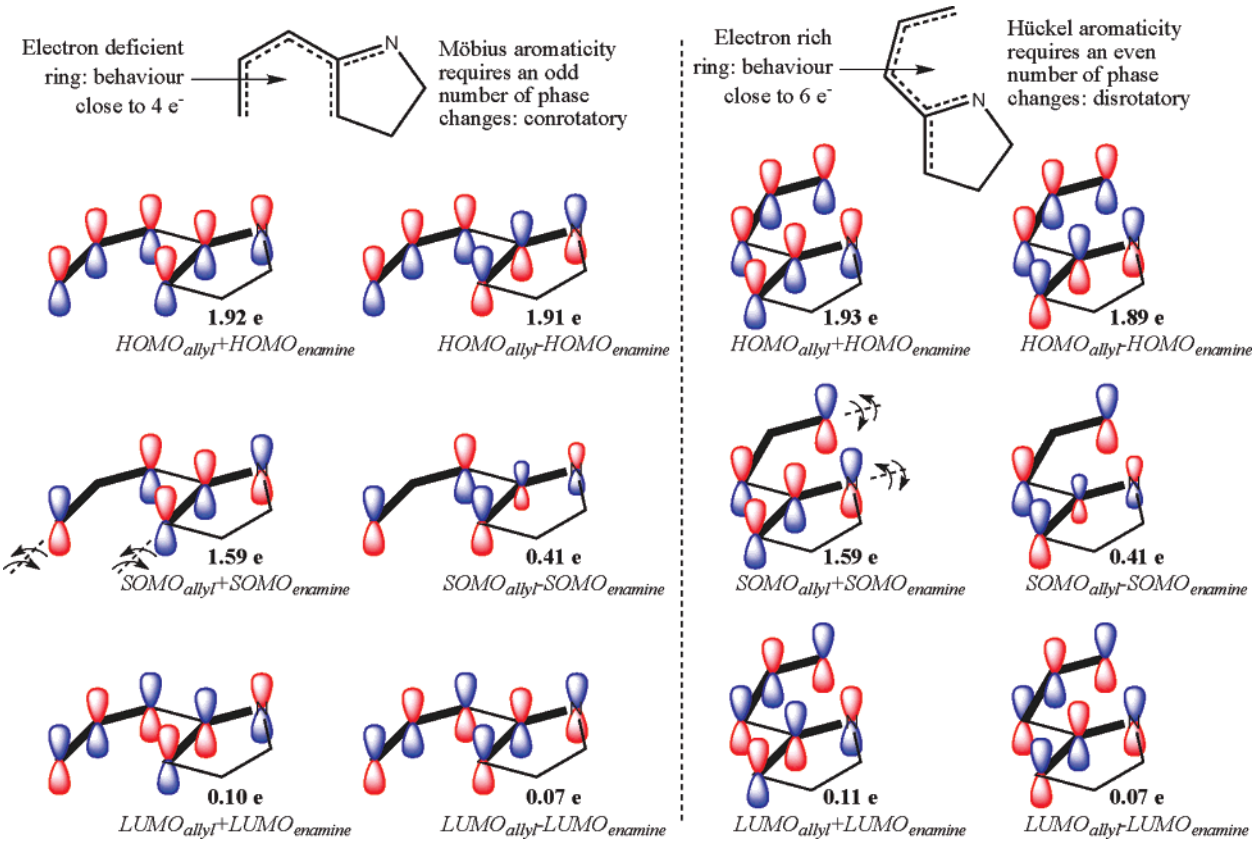

Figure 4. CASSCF natural orbitals of the active space of transition states for the C−C bond-forming cyclization **NC-6a** (left) and C−N bond-forming cyclization **NC-6b** (right). Bold lines indicate the disconnected ally and enamine radicals and the proposed allyl and enamine orbital combinations leading to each natural molecular orbital. Natural orbital populations are also provided to help quantify the diradical character inherent to these species (41% for both **NC-6a** and **NC-6b**, DR = [2 − *n*(HOMO)] × 100).[24]

for reaction. This summary evokes several questions: What is the basis for favoring concerted N_2 extrusion rather than stepwise loss of N_2 via diyl intermediates? What is the basis for the population distribution of **C-5a** and **C-5b**? The lack of equilibration between these two species guarantees that the regiochemistry of product formation will depend only on this ratio. These issues are addressed below.

3.2.2. N_2 Loss. One of the more interesting and unanticipated results from these computational studies emerges from considering the possible pathways for formation of the indole products **19** and **20** from the putative intermediate triazoline **15** (see Figure 6). A priori, three distinct mechanistic manifolds can be envisioned:

- Single C−N or N−N bond scission to furnish intermediate diazo radicals **16a** and **16b**, respectively, followed by loss of nitrogen to deliver the orthogonal singlet diyl **17**. This diyl could cyclize directly via either clockwise or counterclockwise rotation about bond *a* to furnish either the C−C bonded product **19** (counterclockwise) or the C−N bonded product **20** (clockwise).
- Bond *a* rotation within **17** but without bond formation could temporarily park the diyl as the closed-shell indolidenes **(*E*)-18** and **(*Z*)-18**, species which themselves then would cyclize to the observed products **19** and **20**, respectively.
- Concerted elimination of nitrogen (N_2) from **15** to afford the indolidenes **(*E*)-18** and **(*Z*)-18** directly en route to products **19** and **20**.

Transition states for C−N bond cleavage from **15** and concerted loss of N_2 from this same substrate were located. Attempts to identify a transition state corresponding to N−N cleavage within **15** led instead to the same concerted transition state found above. These computational results indicate a strong bias toward concerted loss of N_2 from **15**: $\Delta G^{\ddagger} = 17.4$ kcal/mol for direct **15** → **18** conversion and $\Delta G^{\ddagger} = 25.0$ kcal/mol for **15** → **16a**.

The lower activation barrier for the concerted loss of N_2 from **15** was unexpected, given that this transformation corresponds to a formally disallowed $[10\pi + 2\pi]$ thermal, suprafacial pericyclic retrocycloaddition in the W−H designation. How can this apparent repudiation of the W−H rules be reconciled with the long history of adherence to the same for (retro)cycloaddition processes? The key to understanding this potential disconnect lies in appreciating the orthogonal disposition of the scissile C—N and N—N bonds with the remaining π system. Two additional techniques were applied to illuminate this issue: ACID (anisotropy of the current induced density), which helps visualize delocalization of electron density as might be expected in a concerted (aromatic) bond cleavage/formation process, and NICS (nucleus independent chemical shift), which computes the chemical shift at points in space where there are no nuclei. The ACID representation of the concerted elimination of N_2 from **15** (see Figure 7) indicates that there is essentially no electron density "flowing" between the N═N fragment and the remainder of the (orthogonal) π system at the transition state. Moreover, a quick visual comparison with model Diels−Alder reactions shows evident differences in electron density delocalization at the cleavage points between a Diels−Alder nitrogen cycloreversion and the N_2 extrusion under study here. In addition, the NICS data provide support for this interpretation

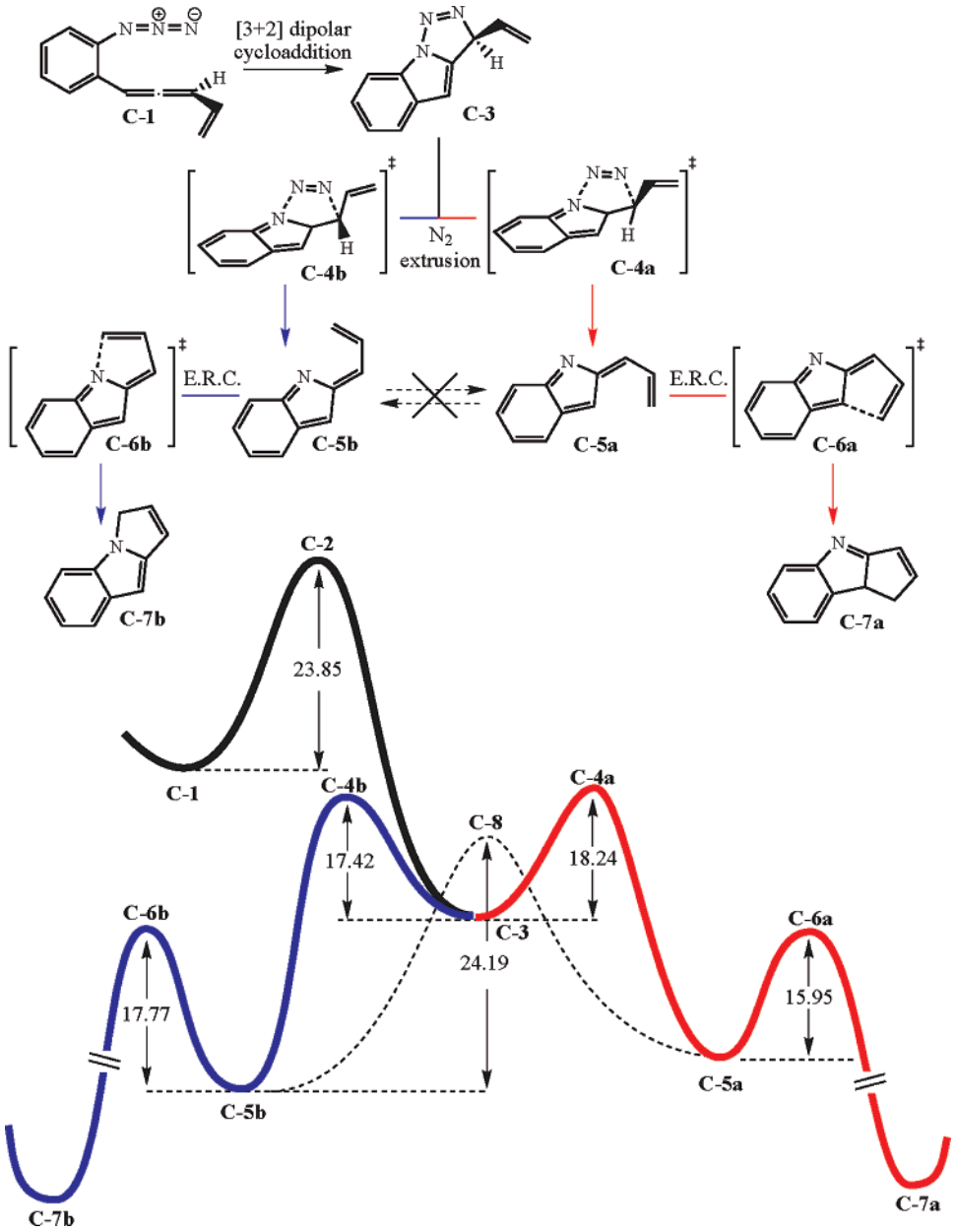

Figure 5. Mechanistic profile for the reaction cascade of conjugated allenyl azides.

by illustrating that there is essentially no shielding effect in the spatial region inside the cleaving ring. For comparison, an analogue calculation on model Diels−Alder and hetero-Diels−Alder reactions (butadiene and ethylene, and butadiene and nitrogen, respectively) reveals a NICS value of ca. 17 ppm. Thus, these calculations suggest that there is no electronic communication between the two halves (N_2 and indole fragment) as the C−C and C−N bonds cleave in a concerted manner, and it is only as the transition state is surmounted that the rotation of bond *a*, which is required to bring the two electronic halves into conjugation, can occur. This "non-least-motion" type of mechanistic pathway, familiar in the chemistry of carbene and ketene cycloadditions, inter alia, then can deliver the closed-shell species **(*E*)-18** and **(*Z*)-18** and then the observed products **19** and **20**, respectively. However, the lack of electronic communication between the two unsaturated fragments at the transition state for bond cleavage places this case outside of the W−H umbrella.

3.2.3. Regioselectivity. The reaction cascade presented in previous work would become a more valuable synthesis methodology if regiocontrol could be achieved. As discussed above, product regiochemistry is determined at the transition state corresponding to N_2 loss, **21** → **22** → **23**, Figure 8. The electronic structure and geometry of transition state **22** was subjected to analysis, leading to the identification of key steric interactions that have the potential to influence the rotational preference of bond *a* (cf. **22a**) and hence the regioisomer distribution of the product. As bond *a* rotates in a counterclockwise direction (illustrated in **22a**, see projection at the top of Figure 8 to distinguish the clockwise and counterclockwise rotations), the steric interaction between R_1 and R_2 diminishes in severity while at the same time the steric interaction between R_1 and the vinyl appendage increases. In contrast, clockwise rotation about bond *a* (cf. **22b**) engenders the opposite steric profile. Therefore, the energetic tradeoff between the burgeoning R_1/vinyl steric interaction in **22a**

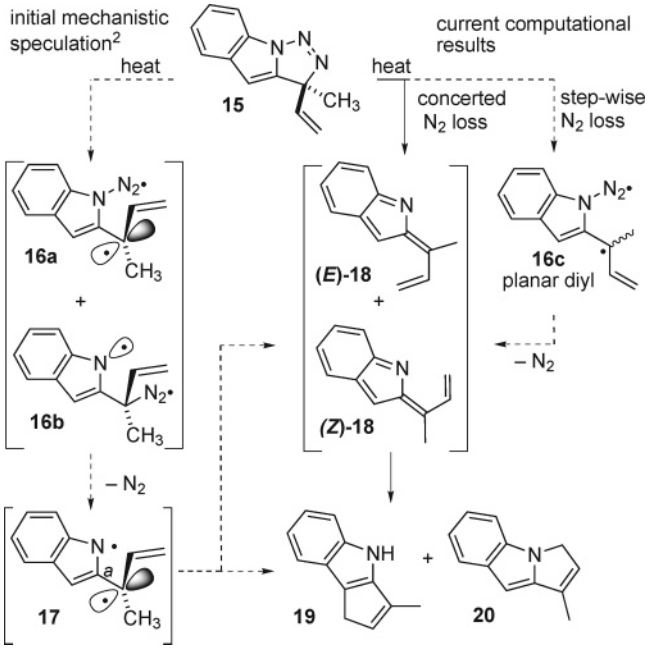

Figure 6. Mechanistic alternatives for the N_2 loss process.

and the similarly increasing R_1/R_2 steric interaction in **22b** should determine the ultimate regioisomer distribution. The experimental data and related computational results presented in Figure 8 bear out this premise. When $R_1 = H$ and $R_2 = CH_3$, there is little difference between the two competing steric interactions, and therefore there is little observed preference between the C−C bonded product **24a** and its C−N bonded alternative **24b**. However, increasing the size of R_2 ($R_1 = H$) leads to a corresponding increase in formation of the C−C bonded product regioisomer **24a**, a result consistent with an increasingly severe $R_1//R_2$ steric penalty in the clockwise rotation of **22b**. The computational results support these observations as well. In the one case ($R_1 = H$, $R_2 = t$-Bu) where both theory and experiment coincide, the calculated result (**24a**/**24b** = 2.8:1 at 110 °C) matches remarkably well with the observed value (**24a**/**24b** = 2.7:1). This encouraging correspondence between calculation and experiment augurs well for the predictive value of this computational methodology. In that vein, if both R_1 and R_2 were non-hydrogen ($R_1 = CH_3$, $R_2 = t$-Bu), selectivities for the C−C bonded regioisomer **24a** greater than 99:1 ($\Delta\Delta G^{\ddagger}$ = 4.4 kcal/mol) would be expected.

3.2.4. Aryl Analogues. The replacement of the terminal vinyl units in **1** and **8** with aryl rings led to a divergence of behavior between the nonconjugated and conjugated systems, Figure 1. The simple nonconjugated aryl derivative **1** behaves similarly to its vinyl counterpart with the exception that it recovers the arene ring's aromaticity through tautomerization following C−C bond formation (compare products **4** and **6** in Figure 1). The aryl substituted *conjugated* substrate $\mathbf{8}_{Ph}$, however, does not undergo C−C bond-forming ring closure upon thermolysis, as does its vinyl analogue. Rather a hydrogen shift intervenes and diverts a putative indolidene intermediate **18** to a 2-styryl indole product **14** (Figure 9). The difference in behaviors between the conjugated and nonconjugated substrates can be attributed to a competition between the relative aromatic resonance energies of the two aryl components within $\mathbf{18}_{Ph}$, a competition that is absent in the nonconjugated series. In **18** the recovery of aromaticity in the indole fragment via electrocyclization provides a strong driving force to provide C−C and C−N bonded products **21** and **22**, respectively (Figure 9). However, in $\mathbf{18}_{Ph}$ this same electrocyclization is accompanied by loss of significant aromatic resonance energy as a new C−C or C−N bond is formed to the arene. The tradeoff between the gain in indolic aromatic resonance energy upon C−C (or C−N) bond formation and the loss of the same at the arene fragment must influence the product distribution. This competition can be resolved by the intervention of a second, independent pathway by which the indole can recapture its aromaticity, but at no expense to

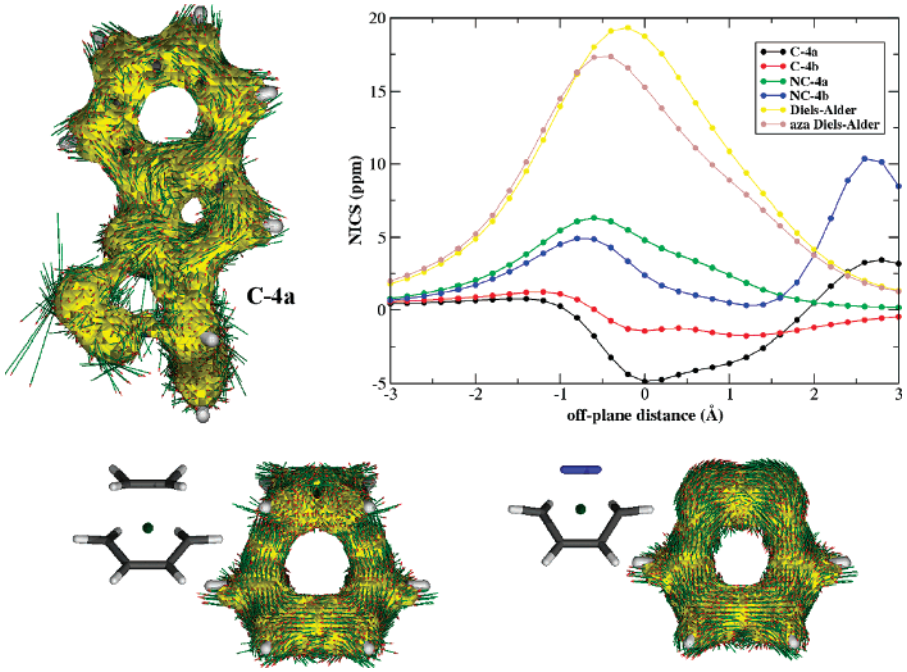

Figure 7. 0.05 au ACID isosurface for the transition state involved in the concerted loss of N_2 **C-4a** and for model Diels−Alder reactions. Plot of the Nucleus Independent Chemical Shift (NICS) for relevant transition states related with the N_2 extrusion.

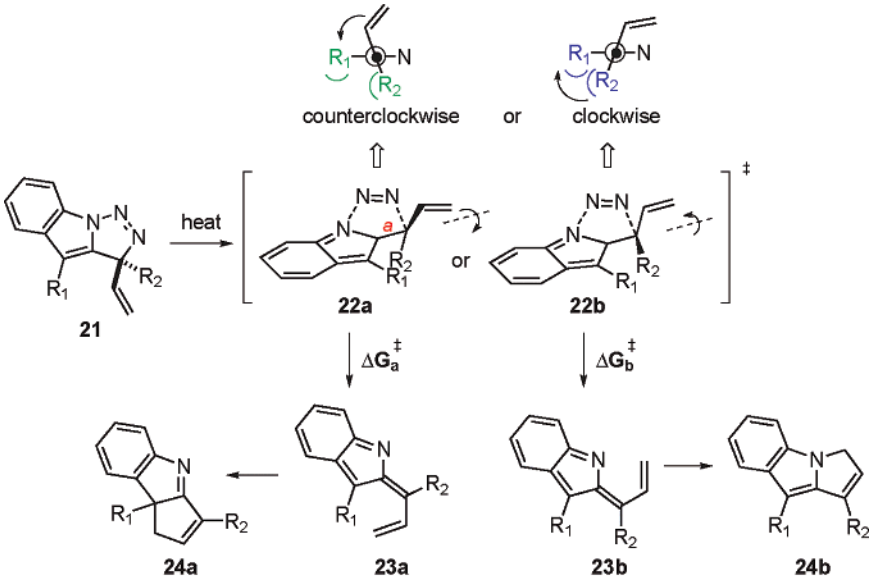

Computational Results

R_1	R_2	$\Delta G_a^{\ddagger} - \Delta G_b^{\ddagger}$
H	H	-0.8
H	*t*-Bu	-0.8
Me	*t*-Bu	-4.4

Experimental Results

R_1	R_2	23a/23b
H	Me	1:1.2
H	CH_2CH_2OTBS	1.5:1
H	*t*-Bu	2.7:1

Figure 8. Computational and previous experimental work on the effect of substitution with bulky groups on regioisomer production. Newman projections of the allene group are included with the transition states, and strong (weak) steric interactions are indicated in blue (green).

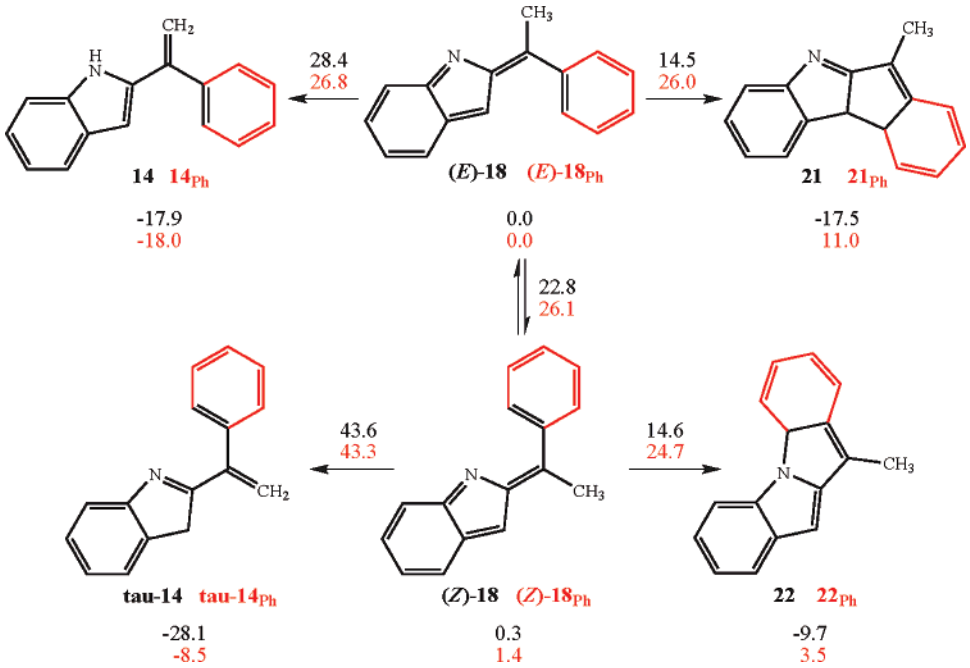

Figure 9. Cyclization pathways for aryl-substituted conjugation disconnected and conjugation connected allene azides.

the arene unit; formal [1,7]-hydrogen shift from the methyl group either to the indolidene's C(3) position (from **(*E*)-18**$_{Ph}$ or to its nitrogen (from **(*Z*)-18**$_{Ph}$) to furnish **14**$_{Ph}$ or its tautomer, tau-**14**$_{Ph}$, respectively. **Tau-14**$_{Ph}$, if formed, then could proceed to the observed product **14** by a simple proton shift.

The calculations support this mechanistic interpretation. The energy barrier for the final C−C bond-forming cyclization of **(*E*)-18**$_{Ph}$ into **21**$_{Ph}$ suffers a severe penalty when compared to its vinyl counterpart (from 14 to 15 kcal/mol (vinyl) to 25−26 kcal/mol (phenyl)). The increase in the electrocyclic ring closure barrier heights for the phenyl-substituted series allows the alternative [1,7]-H shifts to be expressed. The calculated barrier height for the C−H bond forming shift of **(*E*)-18**$_{Ph}$ into **14**$_{Ph}$ at 26.8 kcal/mol is only slightly higher than the calculated **(*E*)-18**$_{Ph}$ → **21**$_{Ph}$ electrocyclization barrier, but the related [1,7] C−H-to-N−H shift extending from **(*Z*)-18**$_{Ph}$, at over 40 kcal/mol, is unlikely to be expressed experimentally. However, the calculated barrier to interconversion of **(*Z*)-18**$_{Ph}$ into **(*E*)-18**$_{Ph}$

(26.1 kcal/mol) is likely to render this isomerization process facile under the experimental conditions.

Thermodynamics also works against C−C bond formation in the phenyl-substituted series. The final product of the ring closure, **21**$_{Ph}$, is thermodynamically unstable with respect to the indolidene intermediate **(*E*)-18**$_{Ph}$ by 11.0 kcal/mol. As a point of comparison, the vinyl-substituted series, with no loss of aromatic resonance energy, exhibits very favorable thermodynamics upon participation in the cyclization (−17.5 kcal/mol for **(*E*)-18** to **21**). Similar numerical values attend the cyclization options of the phenyl- and vinyl-substituted (*Z*)-indolidenes **18** and **18**$_{Ph}$ as well (see Figure 9). Therefore, the mechanistic landscape is open to the interpretation that whereas **(*Z*)-18** and **(*Z*)-18**$_{Ph}$ are probably dead ends, their isomerization to **(*E*)-18** and **(*E*)-18**, respectively, open the possibility that all of the indolidene intermediate is funneled to **21** via electrocyclic ring closure or to **14**$_{Ph}$ via the [1,7]-H shift described above. Both a kinetically accessible pathway to **14**$_{Ph}$ and a large thermodynamic disincentive to form **21**$_{Ph}$ and **22**$_{Ph}$ guide the chemistry of the intermediate indolidene **18**$_{Ph}$.

4. Conclusion

Several questions regarding the mechanistic intricacies of the allenyl azide cyclization cascade were posed in the Introduction. The computational results reported herein address and clarify all of these issues. The primary question of C−C vs C−N bond formation appears to hinge on the distinct nature of the key intermediates. The nonconjugated system appears to proceed through an intermediate diyl that favors C−C bond-forming cyclization at the more electron-rich carbon radical site, whereas the conjugated system progresses through closed-shell indolidene alkene isomers whose ultimate fate (C−C or C−N bond formation) is determined by the (*E*)/(*Z*) alkene isomer ratio. In the conjugated substrate series, a diyl intermediate was not found along the reaction coordinate, emphasizing the mechanistic dissimilarity between the reactions of the conjugated and nonconjugated allenyl azides. The diyls that are formed from the nonconjugated substrates cyclize with complete stereochemical control through a five-electron conrotatory process resembling the familiar 4*n*-type W−H electrocyclizations. Finally, the competition between electrocyclization and [1,7]-hydrogen shift within the conjugated system-derived indolidene depends on the nature of the terminal unsaturation; if an alkene is present, electrocyclization is preferred energetically and tricyclic product is formed, whereas if the terminal unsaturation is an arene ring, disrupting its aromaticity is too penalizing, and the [1,7]-H shift predominates. Overall, these results point to the value of computational approaches in disentangling complex reaction sequences that may feature bis allylic diradicals. The DFT-based approach appears robust and has the potential to guide future experimental research by offering testable predictions on issues of selectivity.

Acknowledgment. The authors are grateful to CESGA for allocation of supercomputer time. Funding from the Institute of General Medical Sciences of the National Institutes of Health (GM 72572) to K.S.F. is gratefully acknowledged.

Supporting Information Available: Cartesian coordinates and SCF energies of all the computed molecules, further calculations to check the methodology employed, and the full citation for ref 9. This material is available free of charge via the Internet at http://pubs.acs.org.

JA070818L